

[Supporting Information]

One-Step Synthesis of Au@Pd Core-Shell Nanooctahedron

Young Wook Lee,^{†,‡} Minjung Kim,^{†,‡} Zee Hwan Kim,[§] and Sang Woo Han^{*,†}

[†] *Department of Chemistry and KI for the NanoCentury, KAIST, Daejeon 305-701, Korea*

[‡] *Environmental Biotechnology National Core Research Center, Gyeongsang National University, Jinju 660-701, Korea*

[§] *Department of Chemistry, Korea University, Seoul, 136-701, Korea*

*Corresponding author. *E-mail:* sangwoohan@kaist.ac.kr

Experimental

Chemicals and Materials. HAuCl₄ (Aldrich, 99.99+%), K₂PdCl₄ (Aldrich, 99.99%), cetyltrimethylammonium chloride (CTAC, Aldrich, solution in water, 25 wt%), and 1,4-phenylene diisocyanide (1,4-PDI, Aldrich, 99%) were all used as received. Other chemicals, unless specified, were reagent grade, and Milli-Q water with a resistivity of greater than 18.0 MΩ·cm was used in the preparation of aqueous solutions.

Preparation of Nanoparticles. In a typical synthesis of Au-Pd bimetallic nanoparticles, 1 mL of a 5 mM aqueous solution of HAuCl₄/K₂PdCl₄ mixtures in molar ratios of 3:1, 1:1, and 1:3 was added to 5 mL of 50 mM CTAC. The whole system was sealed, heated, and maintained at 90 °C in a conventional forced-convection drying oven for 48 h. The concentrations of CTAC have no influence on the shape of resultant particles. We have obtained almost identical octahedral particles with different concentration of CTAC solutions (10-100 mM). The resulting hydrosol was subjected to centrifugation (9000

rpm for 5 min) to remove excess CTAC. For comparison, Au and Pd monometallic nanoparticles were prepared in the same way by substituting aqueous solutions of H₂AuCl₄/K₂PdCl₄ mixtures by H₂AuCl₄ and K₂PdCl₄ solutions, respectively. Hereafter, we will refer to the metal nanoparticles prepared from the aqueous solutions of H₂AuCl₄/K₂PdCl₄ mixtures in molar ratios of 3/1, 1/1, and 1/3 as Au₃Pd₁, Au₁Pd₁, and Au₁Pd₃, respectively.

Characterization of Nanoparticles. The extinction spectra were recorded with a UV-vis absorption spectrometer (Agilent 8453). Scanning electron microscopy (SEM) images of the samples were taken with a field-emission scanning electron microscope (FESEM, Phillips Model XL30 S FEG). Transmission electron microscopy (TEM) images were obtained with a JEOL JEM-2010 transmission electron microscope operating at 200 kV after placing a drop of hydrosol on carbon-coated Cu grids (200 mesh). High-resolution TEM (HRTEM) and high-angle annular dark-field scanning TEM (HAADF-STEM) characterizations were performed with a FEI Technai G2 F30 Super-Twin transmission electron microscope operating at 300 kV. The effective electron probe size and dwell time used in HAADF-STEM-EDS mapping experiments were 1.5 nm and 200 ms per pixel, respectively. The compositions of Au-Pd bimetallic nanoparticles were determined by inductively coupled plasma mass spectrometry (ICP-MS ELAN 6000, Perkin-Elmer). X-ray diffraction (XRD) patterns were obtained with a Bruker AXS D8 DISCOVER diffractometer using Cu K α (0.1542 nm) radiation. FT-IR spectra were measured by using a Bruker Equinox 55 FT-IR spectrometer. Raman spectra were obtained using a Jobin Yvon/HORIBA LabRAM spectrometer equipped with an integral microscope (Olympus BX 41). The 632.8 nm line of an air-cooled He/Ne laser was used as an excitation source. Raman scattering was detected with 180° geometry using a thermoelectrically cooled 1024 \times 256 pixel charge coupled device (CCD) detector. The Raman band of a silicon wafer at 520 cm⁻¹ was used to calibrate the spectrometer. For Raman measurement, drop-casting film of nanoparticles on Si substrate was soaked in 0.1 mM 1,4-PDI solution in ethanol overnight. After the substrate was taken out, it was washed with ethanol and dried under ambient condition.

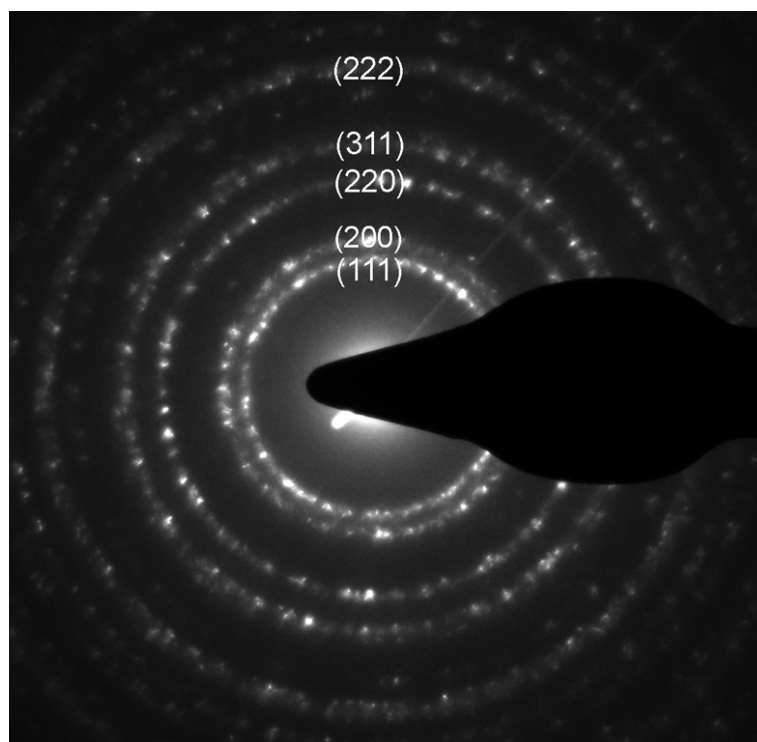


Figure S1. Selected area electron diffraction (SAED) pattern of the Au@Pd core-shell nanooctahedra. The observed diffraction rings can be assigned to the (111), (200), (220), (311), and (222) diffractions of metal with face-centered cubic (fcc) structure.

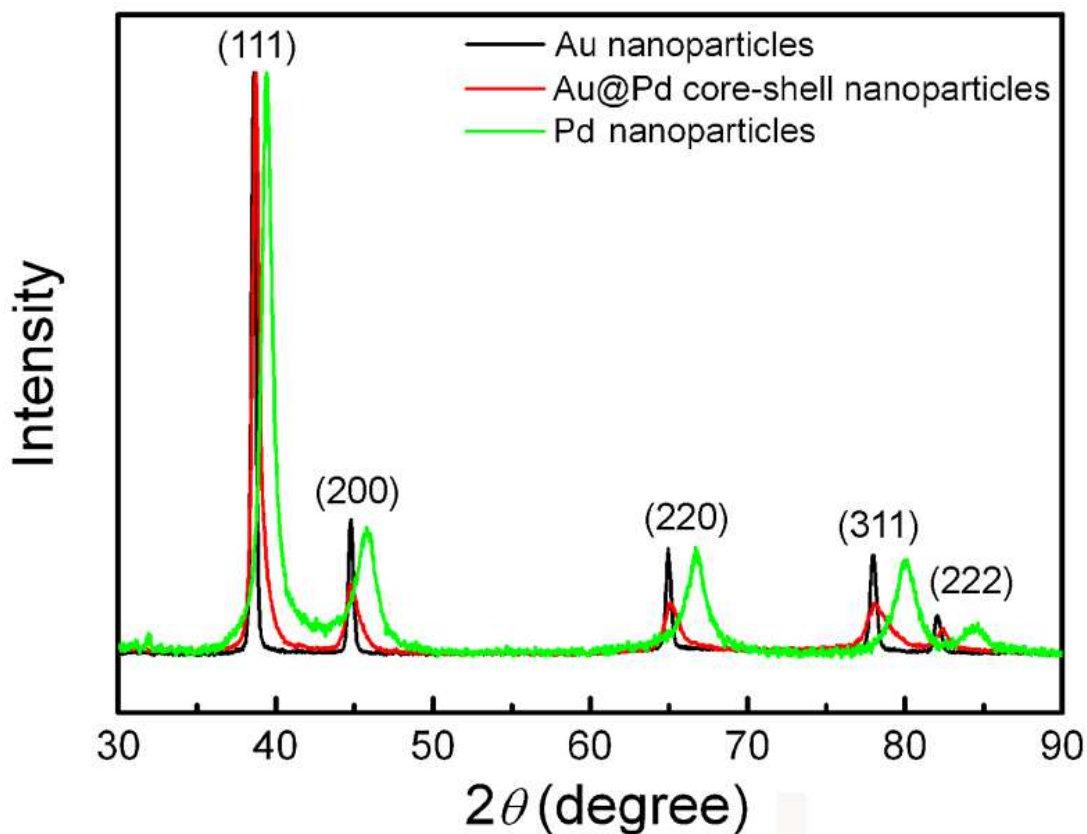


Figure S2. X-ray diffraction (XRD) pattern of the Au@Pd core-shell nanoparticles. For comparison, XRD patterns of monometallic Au and Pd nanoparticles are also shown. Observed five peaks can be indexed to the (111), (200), (220), (311), and (222) reflections of face-centered cubic (fcc) structure of metal, showing the pure crystalline nature of the prepared particles. Peak positions of core-shell nanoparticles are similar with those of Au nanoparticles. Since the thickness of Pd shell is too thin to give rise to distinct diffraction peaks.^{S1} However, shoulder peaks were observed for each diffraction peak, which can be attributed to Pd.

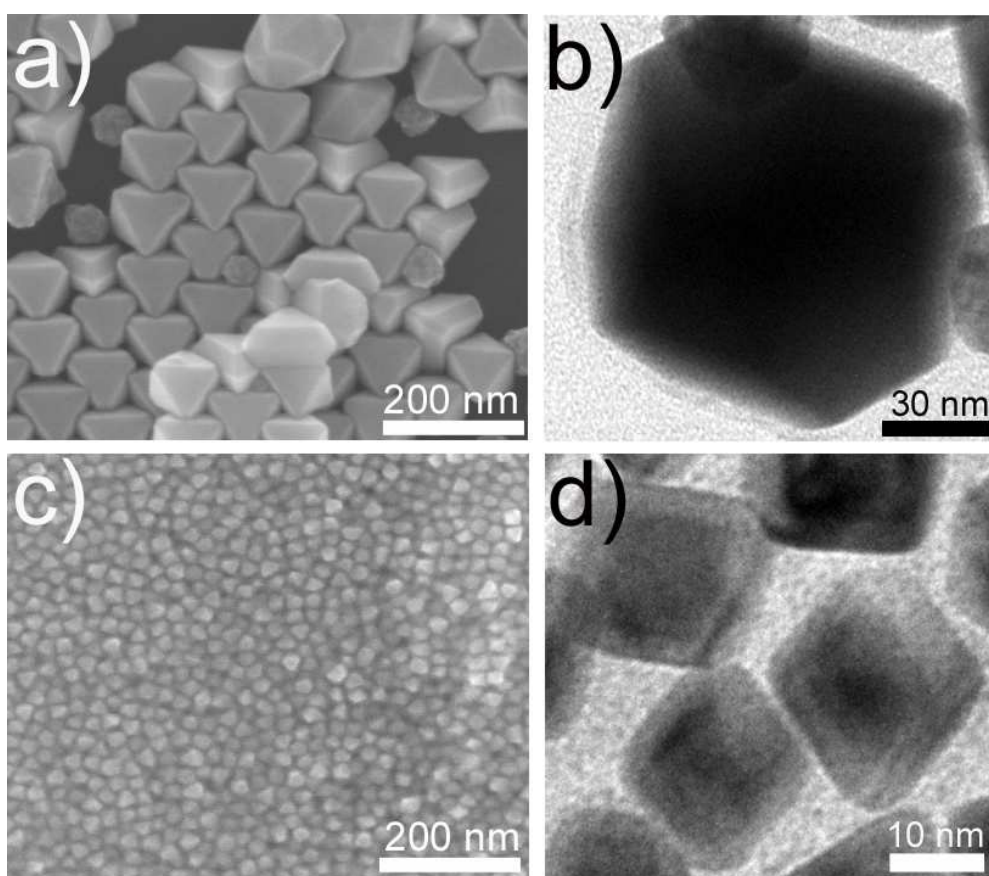


Figure S3. SEM (a) and TEM (b) images of the bimetallic Au-Pd nanoparticles prepared from the aqueous solution of $\text{HAuCl}_4/\text{K}_2\text{PdCl}_4$ mixture in molar ratio of 3:1. SEM (c) and TEM (d) images of the Au-Pd nanoparticles prepared from the $\text{HAuCl}_4/\text{K}_2\text{PdCl}_4$ mixture in molar ratio of 1:3. The measured mean edge lengths of Au-Pd nanoparticles prepared from the $\text{HAuCl}_4/\text{K}_2\text{PdCl}_4$ mixtures in molar ratios of 3:1 and 1:3 are 81.1 ± 6.1 and 17.5 ± 1.1 nm, respectively. The interesting finding is that the Pd shell thicknesses of Au@Pd nanoparticles are essentially unchanged regardless of their compositions and sizes; 5.6 ± 0.9 , 5.6 ± 0.8 , and 5.1 ± 0.6 nm for Au_3Pd_1 , Au_1Pd_1 , and Au_1Pd_3 , respectively. Although the exact mechanism is still under investigation, the observed composition-independent shell thicknesses indicate that there may be a certain limiting mechanism for the growth of Pd shell on the Au core associated with inefficient reduction of Pd precursor under our experimental condition.

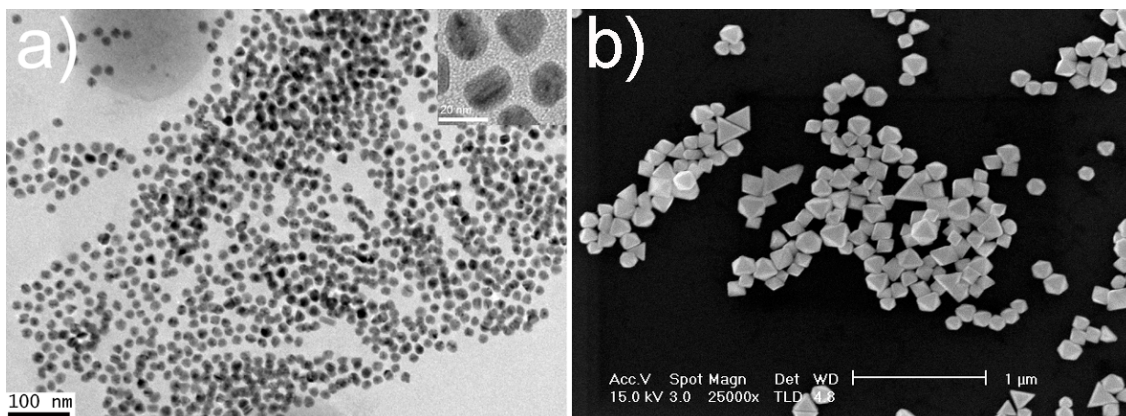


Figure S4. (a) TEM image of monometallic Pd nanoparticles. (b) SEM image of monometallic Au nanoparticles. The Pd and Au nanoparticles were synthesized by using pure Pd and pure Au precursors, respectively.

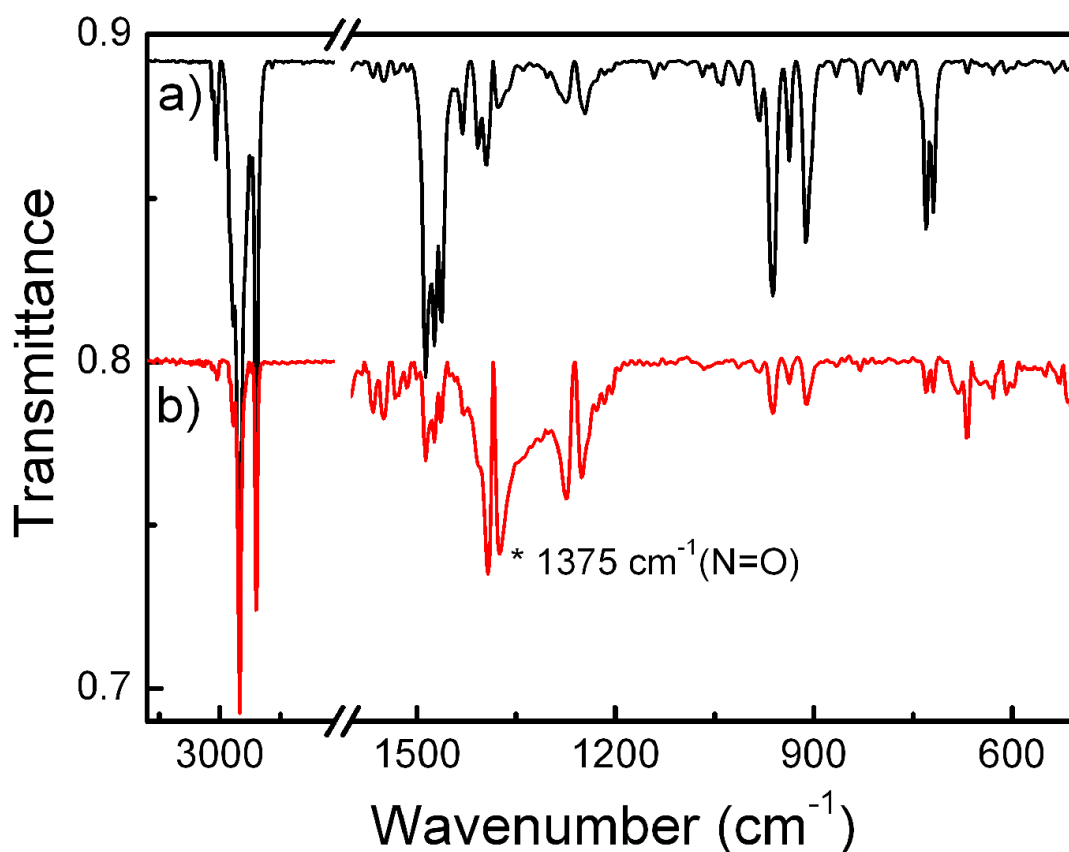


Figure S5. FT-IR spectra of (a) original CTAC and (b) CTAC-stabilized Au@Pd nanoparticles. Although a slight shift of peak position is observed, FT-IR spectrum of CTAC-stabilized nanoparticles is similar with that of the CTAC. The noticeable difference between two spectra is the appearance of a new peak at 1375 cm^{-1} in the spectrum of CTAC-stabilized nanoparticles, which can be assigned to N=O vibration.^{S2} This indicates that the nitroso group has been produced after reaction through the oxidation of CTAC. The observed peak positions and their assignments are summarized in Table S1.

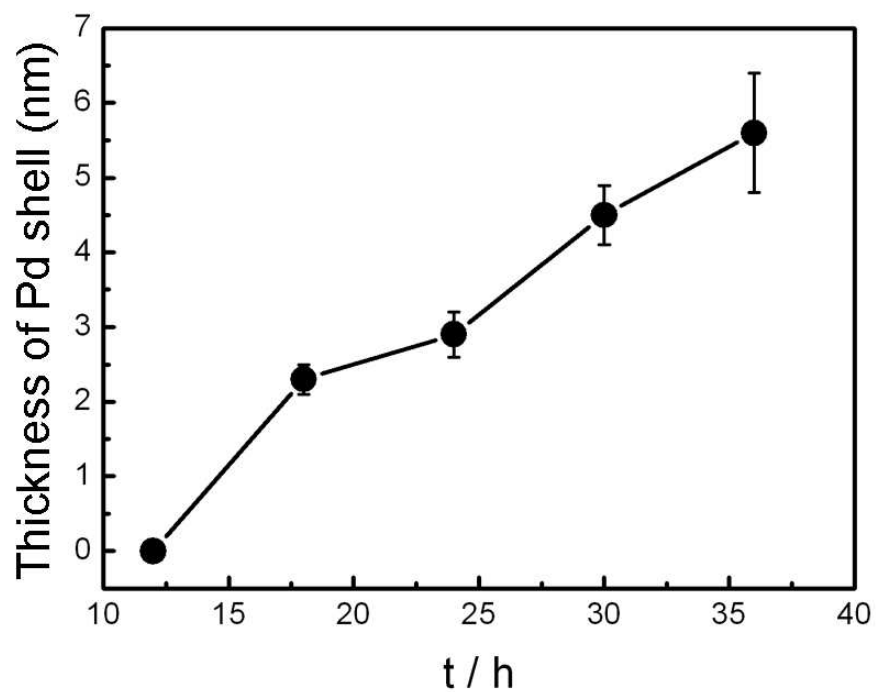


Figure S6. Change in the Pd shell thickness during the reaction estimated from TEM analysis.



Figure S7. Photographs of reaction solution reacted under different reaction times.

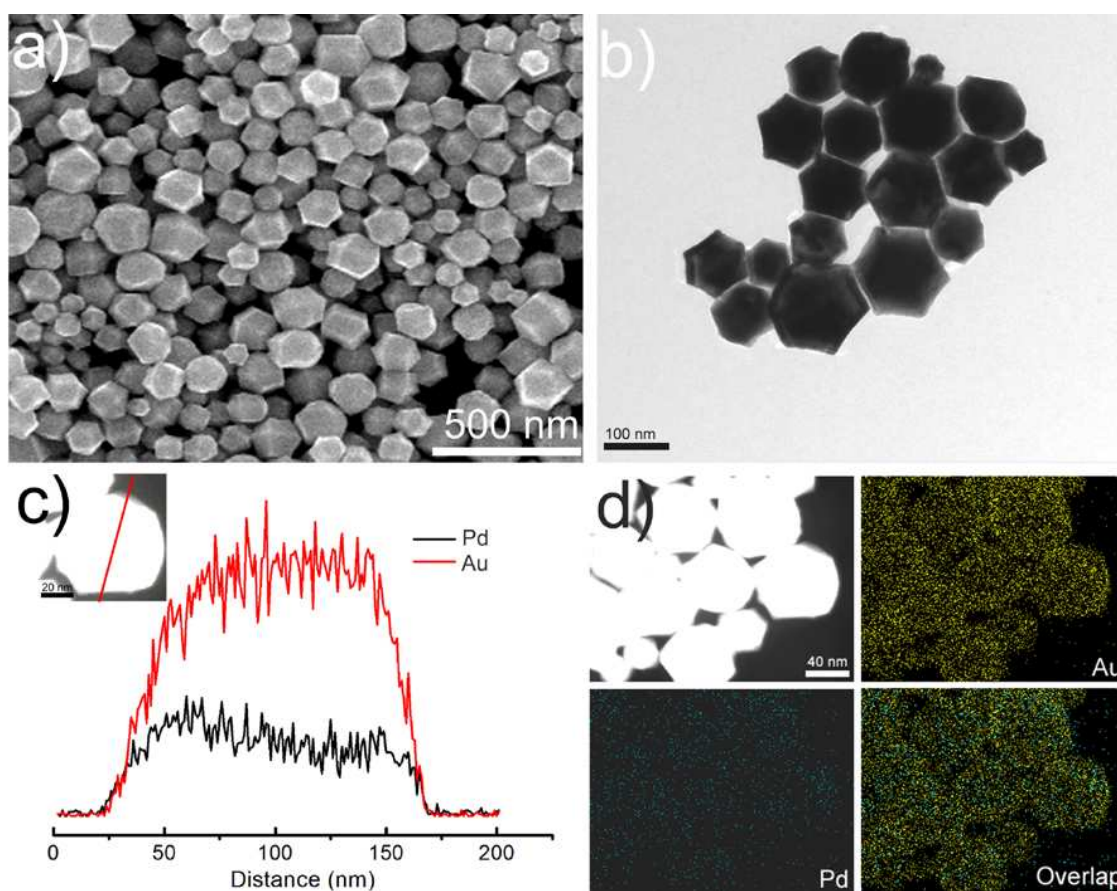


Figure S8. SEM (a) and TEM (b) images of the Au-Pd bimetallic nanoparticles prepared in the presence of ascorbic acid (50 μ L, 100 mM). (c) HAADF-STEM image and cross-sectional compositional line profiles of an Au-Pd bimetallic nanoparticle. (d) HAADF-STEM-EDS mapping images of the Au-Pd nanoparticles. All electron microscopic data clearly show that homogeneously alloyed Au-Pd nanoparticles are formed by using ascorbic acid as a reducing agent. Close inspection of microscopic images reveals that the majority of the particles are rhombic dodecahedra (\sim 65 %). Other shapes include square bipyramid (\sim 12 %), regular dodecahedra (\sim 8 %), and ill-defined polyhedra (\sim 15 %).

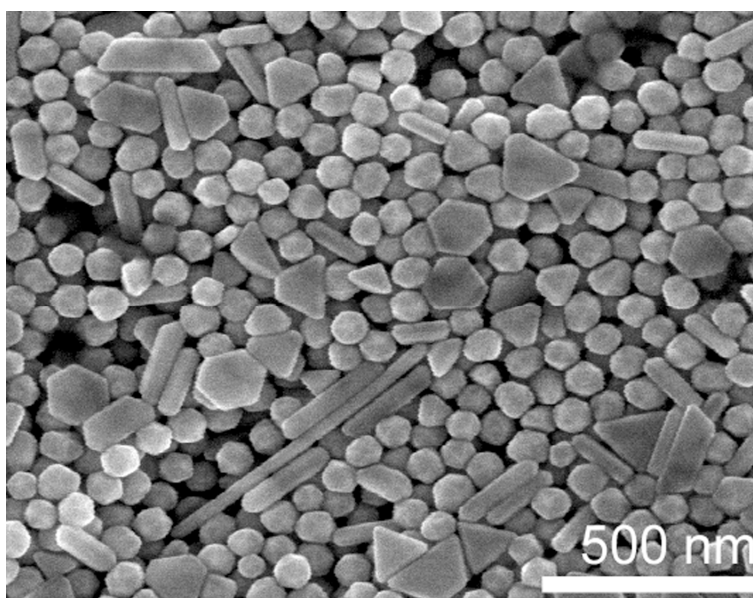


Figure S9. SEM image of the Au-Pd bimetallic nanoparticles prepared with cetyltrimethylammonium bromide (CTAB, Sigma, $\geq 98\%$).

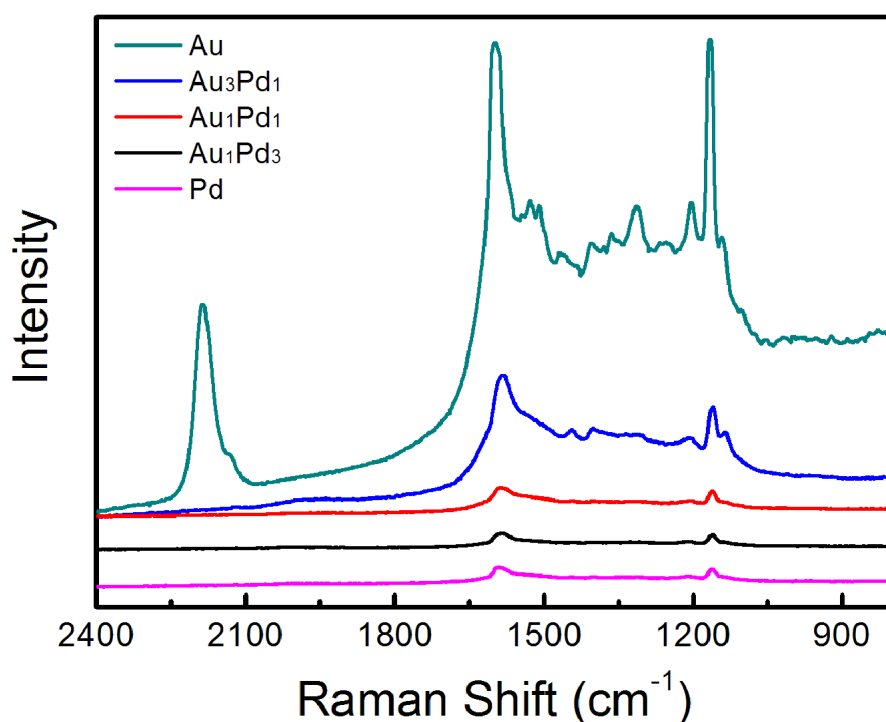


Figure S10. Surface-enhanced Raman scattering (SERS) spectrum of 1,4-phenylene diisocyanide (1,4-PDI) adsorbed on Au@Pd nanooctahedra and monometallic Au and Pd nanoparticles. It is well known that arylisocyanide molecules such as 1,4-PDI adsorb on metal substrates via different mechanism as the kind of metal and such structural differences can readily be detected by SERS. The observed SERS spectral features of the particles are almost identical with that obtained by monometallic Pd nanoparticles.^{S3} Together with the UV-vis spectral observations, this is the spectroscopic evidence of the complete coating of Pd shell. It is noticeable that the SERS intensity from the Au₃Pd₁ particles is remarkably higher than those from other bimetallic particles. Considering the ineffective damping of SPR of Au core in the case of Au₃Pd₁ sample (Figure S11), the enhanced SERS signal obtained with Au₃Pd₁ particles can be the result of the long-range effect of the strong electromagnetic field created by the high SERS-active Au core underneath.^{S4}

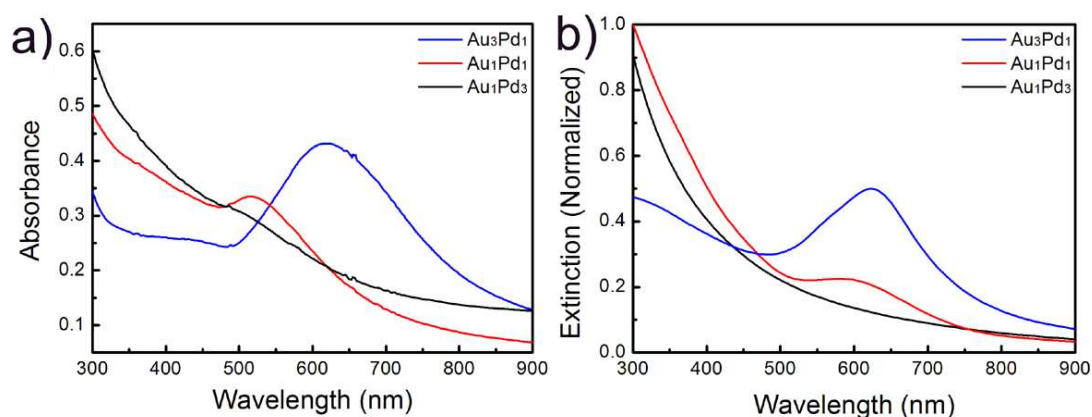


Figure S11. The metal nanoparticles with specific geometrical shapes exhibit distinct plasmon absorption that is dependent on their sizes and shapes.^{S5} Figure S11a shows the extinction spectra of the as-prepared Au@Pd octahedral particles in water, which shows the single surface plasmon resonance (SPR) peak that can be assigned to the dipole resonance of Au core.^{S6} In addition, as the relative content of Pd is increased (i.e., reduction of core size while keeping the Pd shell thickness constant (see Figure S3)), the SPR peak of Au-core quickly fades away. As is previously reported,^{S4} shells of Pd or Pt strongly damp out the dipolar plasmon oscillations of Au or Ag cores, because Pd or Pt have significantly lower conductivities at optical frequency than those of Au or Ag. As such, increase in shell thickness progressively damps out the SPR peak of the core. In our case, similarly, the shell thicknesses of the particles are kept constant, while the size of the core is reduced, which increasingly damps out the plasmon resonance of the Au core. To confirm our interpretation of the spectra, the spectra have been simulated using the 3-dimensional finite difference time domain (FDTD) method^{S7} with the commercial FDTD-Lumerical™ simulation package. The frequency-dependent dielectric constants of Au and Pd have been taken from the literature,^{S8} and the refractive index of surrounding water ($n = 1.33$) has been taken into account. The calculation employs the perfectly matched layer (PML) boundary conditions, and the spectra are obtained by the total-field scattered-field (TFSF) technique that selectively isolates the incident and scattered field components. The geometric models for Au₃Pd₁, Au₁Pd₁, and Au₁Pd₃ particles were constructed based on the experimentally observed structural parameters (core size and shell thickness). As can be seen in Figure S11b, the simulation faithfully reproduces essential features of the experimental spectra, which further confirms the influence of highly damping shells on the plasmon resonances of the core. The some differences in SPR peak positions and shapes between observed and calculated spectra can be ascribed to the size distribution of the prepared particles.

Table S1. IR peaks (cm^{-1}) assignments for CTAC and CTAC-stabilized Au@Pd nanoparticles.

CTAC	Au@Pd -CTAC	Assignments ^{S2,S9}
3020	3011	$\text{CH}_{3\text{asym}} (-\text{N}+(\text{CH}_3)_3)$
2944	2944	$\text{CH}_{3\text{sym}}(-\text{N}+(\text{CH}_3)_3)$
2915	2917	$\text{CH}_{2\text{asym}}$
2854	2949	$\text{CH}_{2\text{sym}}$
1486	1486	$\delta(\text{CH}_3)_{\text{asym}}$
1473	1473	$(\text{CH}_2)_{\text{def}}$
1462	1462	$(\text{CH}_2)_{\text{sciss}}, \delta(\text{N}^+\text{CH}_3)_{\text{sym}}$
1406	1406	
1394	1392	
	1375	$\text{N}=\text{O}$
962	961	CN^+
937	936	
911	910	
730		
719	668	$\text{CH}_{2\text{rock}}$

References

- (S1) Nakagawa, T.; Nitani, H.; Tanabe, S.; Okitsu, K.; Seino, S.; Mizukoshi, Y.; Yamamoto, T. A. *Ultrason. Sonochem.* **2005**, *12*, 249.
- (S2) Chen, H.; Wang, Y.; Dong, S. *Inorg. Chem.* **2007**, *46*, 10587.
- (S3) Y. W.; Kim, N. H.; Lee, K. Y.; Kwon, K.; Kim, M.; Han, S. W. *J. Phys. Chem. C* **2008**, *112*, 6717.
- (S4) Tian, Z.-Q.; Ren, B.; Li, J.-F.; Yang, Z.-L. *Chem. Commun.* **2007**, 3514.
- (S5) Noguez, C. *J. Phys. Chem. C* **2007**, *111*, 3806.
- (S6) (a) Heo, J.; Kim, D.-S.; Kim, Z. H.; Lee, Y. W.; Kim, D.; Kim, M.; Kwon, K.; Park, H. J.; Yun, W. S.; Han, S. W. *Chem. Commun.* **2008**, 6120. (b) Kim, D.; Heo, J.; Kim, M.; Lee, Y. W.; Han, S. W. *Chem. Phys. Lett.* **2009**, *468*, 245.
- (S7) Oubre, C.; Nordlander, P. *J. Phys. Chem. B* **2004**, *108*, 17740.
- (S8) Palik, E. D., Ed.; *Handbook of Optical Constants of Solids*; Academic Press: New York, 1991.
- (S9) Borodko, Y.; Jones, L.; Lee, H.; Frei, H.; Somorjai, G. *Langmuir* **2009**, *25*, 6665.